2022-01-0271 Published 29 Mar 2022

An Experimental Study of In-Cylinder Heat Transfer from a Pressurized Motored Engine with Varying Peak Bulk Gas Temperatures

Carl Caruana and Mario Farrugia University of Malta

Gilbert Sammut Dolphin N2 Limited

Emiliano Pipitone University Of Palermo

Citation: Caruana, C., Farrugia, M., Sammut, G., and Pipitone, E., "An Experimental Study of In-Cylinder Heat Transfer from a Pressurized Motored Engine with Varying Peak Bulk Gas Temperatures," *SAE Int. J. Advances & Curr. Prac. in Mobility* 4(5):1747-1761, 2022, doi:10.4271/2022-01-0271.

This article was presented at the WCX World Congress Experience, April 5-7, 2022.

Received: 08 Oct 2021 Revised: 26 Dec 2021 Accepted: 13 Jan 2022

Abstract

The variation of in-cylinder heat transfer with parameters such as engine speed, air-to-fuel ratio, coolant temperature and compression ratio were frequently studied in classical research. These experimentally-obtained relationships are important for improving in-cylinder heat transfer models, essential in developing CO_2 reducing strategies. In this publication, a 2.0 liter compression ignition engine was tested in the pressurized motored configuration. This developed experimental setup allowed testing of the engine at speeds ranging between 1400 rpm and 3000 rpm, with peak in-cylinder gas pressures from 40 bar to 100 bar. The engine was motored using different gas compositions chosen specifically to have ratios of specific heats of 1.40, 1.50, 1.60 and 1.67 at room temperature. This enabled motored testing with peak in-cylinder bulk gas temperatures ranging from 700 K to 1500 K. This wide variation of peak bulk gas temperature was achievable even at constant peak in-cylinder gas pressure, which gave the possibility of varying the thermal load of the engine independently from the gas pressure load. This experimental setup offered the repeatability and robustness of motored testing, with the benefit of a fired-representative gas pressure and thermal load. Throughout the test matrix, the engine was instrumented with eroding surface thermocouples at two locations in the cylinder head; at the cylinder central axis, and at the periphery in the squish region. The steady-state and transient components of heat flux were investigated separately, along with the average surface temperature and its swing. The transient component of heat flux was computed using the Impulse Response method, coupled with a two-dimensional finite element model of the eroding thermocouples, as presented in SAE 2021-24-0018. This method takes into account the two-dimensional nature of heat flux through the thermocouples and hence presents a more robust analysis than the more common one-dimensional treatment using the Fast-Fourier Transform method.

Introduction

In modern times, the capability of the internal combustion engine is still not met by alternative mobility technologies in sectors such as the construction or naval industries which require on-demand and reliable high-power delivery, without compromising payload or downtime for charging. This requires high-density energy input which at present is only available from hydrocarbon fuels. Hence, the quest to optimize the engine structure and reduce emissions is still vital. In-cylinder heat transfer is the main cause that impedes improvement of the internal combustion engine. Proposal of new solutions to reduce heat transfer are often hindered by the difficulty of measurement and understanding of heat transfer and its interactions. Researchers tried to understand the complex mechanisms of heat transfer since the early years of the IC engine [1]. Despite these efforts, experimental measurements of in-cylinder heat transfer still remain very challenging to obtain with good fidelity. This challenge makes it difficult to characterize the behavior of heat transfer with important engine design parameters (compression ratio, combustion chamber shape, cylinder dimensions, in-cylinder flow structure) and operating variables (engine speed, in-cylinder pressure load, coolant and gas temperature). As a result, predictive models used at the early stages of engine design based on these characterizations, are often inaccurate and not representative of actual engine phenomena.

Several attempts have been made to improve the robustness of in-cylinder heat transfer measurements, with some of which proposing new measurement [2] or processing methods [3, 4, 5]. The most frequently used method for in-cylinder heat

transfer determination still remains that which is based on the spectral analysis of the measured surface temperature swing [6, 7, 8]. This method uses a fast response thermometer, often being a thermocouple, which has to be integrated at the surface of the instrumented component; either the cylinder head or the piston crown. This method of in-cylinder heat transfer measurement has several shortcomings which are well known in this research field. First and foremost, it is only capable of giving a point measurement of where the thermocouple is installed; hence to have a clear indication of the overall heat transfer, several of these thermocouples would have to be fitted across the combustion chamber. This is hindered by the intrusiveness of fitting these thermocouples, which often requires custom drilling through the cylinder head, and hence makes their fitment quite challenging. The in-service lifetime of the thermometers is not long, especially at harsh operating conditions, which requires very frequent maintenance. Furthermore, if the engine is tested in the fired condition, soot deposition on the surface thermometer would significantly slow down its response time. One of the most problematic and error-prone characteristic of this measurement method is that the majority of these surface thermometers are made up of several materials. This gives rise to multi-dimensional heat transfer within the thermometer, which complicates the computation of the heat transfer from the surface temperature swing. In past research, several authors have tried to minimize the multi-dimensionality of the thermocouple setup and assumed the heat transfer through the thermometer to resemble that of a one-dimensional, semi-infinite solid [6, 7, 8]. Other authors tried to account for the multi-dimensional effects and proposed new methods, either based on a finite difference calculation [9], or the Impulse Response method [3, 4]. The above presented shortcomings of the surface temperature measurement method were discussed in detail by the same authors of this publication in [10]. Solutions to the presented shortcomings were also proposed.

The aim of this research paper is to present the experimentally obtained results of the surface temperature swing at the cylinder head surface and the computed heat transfer that were obtained from an extensive test matrix. In the following sections, the experimental apparatus will first be presented, followed by a brief explanation of the method used to obtain the in-cylinder heat transfer from the surface temperature measurement. An overview of the test campaign is then presented. Finally, the results of the surface temperature and in-cylinder heat transfer are presented and discussed. Although not strictly necessary, the reader will benefit if [10] is consulted first before reading this paper.

Experimental Apparatus

This study was conducted on a single cylinder version of an inline four-cylinder, 2.0 liter engine. The conversion of the engine from four cylinders to single cylinder is detailed in [11]. The experimental setup was operated in the pressurized motored configuration, which allowed engine speeds ranging between 1400 rpm and 3000 rpm and peak in-cylinder gas pressures from 40 bar to 100 bar.

TABLE 1 Engine specifications.

Make and Model	Peugeot 306 2.0L HDi
Year of Manufacture	2000
Number of Strokes	4-stroke
Number of Cylinders	4, 3 deactivated, 1 active
Valvetrain	8 Valve, OHC
Static Compression Ratio	18:1
Engine Displacement [cc]	1997
Bore [mm]	85
Stroke [mm]	88
Connecting Rod Length [mm]	145
Intake Valve Diameter [mm]	35.6
Exhaust Valve Diameter [mm]	33.8
Intake Valve Opens (1mm lift)	10 CAD ATDC intake
Intake Valve Closes (1mm lift)	20 CAD ABDC intake
Exhaust Valve Opens (1mm lift)	45 CAD BBDC expansion
Exhaust Valve Closes (1mm lift)	10 CAD BTDC exhaust

The pressurized motored method involves motoring the engine with an electric motor, whilst pressurizing its intake (conventionally with air). Intake air pressures up to 2.5 bar can reach fired-like peak in-cylinder pressures of up to 140 bar, depending on the compression ratio and the intake manifold pressure. To recycle the exhausted air, a shunt pipe was introduced between the intake and exhaust manifolds, which recirculated the exhaust gas back to the intake manifold. The engine specifications are given in Table 1.

The engine was operated using air, argon and two mixtures involving both constituents. This gave the ability to vary the peak of the in-cylinder gas temperature from 700 K to 1500 K without changing the engine speed or gas pressure load, something which cannot be easily achieved from a fired setup. The same motored experimental setup with intake manifold pressurization and recirculation using the shunt pipe was first used in [12], using only air, and was later modified to operate with argon and its mixtures with air in [13, 14, 15]. A photo of the experimental setup is shown in Figure 1.

To conduct the in-cylinder surface temperature measurements, the cylinder head combustion chamber surface was instrumented at two locations using surface thermocouples of the eroding type. One surface thermocouple was fitted in place of the OEM injector, and the other surface thermocouple was fitted at a custom-drilled location in the cylinder head, which coincides with the squish region at the periphery of the cylinder. The two instrumented locations on the cylinder head surface, and the corresponding locations on the piston are shown in Figure 2 and Figure 3 respectively. It should be noted that the surface thermocouple at the custom-drilled location was fitted flush and perpendicular to the cylinder head surface, while the thermocouple at the OEM injector location had to be mounted with its surface protruding by 0.7 mm from the surface of the cylinder head and slightly inclined to the vertical, due to the inclination of the OEM injector hole. Since it is not ideal to have the surface thermocouple protruding from the cylinder head surface, data from this thermocouple will be less referred to in this publication.

FIGURE 1 The pressurized motored experimental setup. Note the circular loop connecting the intake and exhaust manifolds that are located on the same side of the cylinder head.

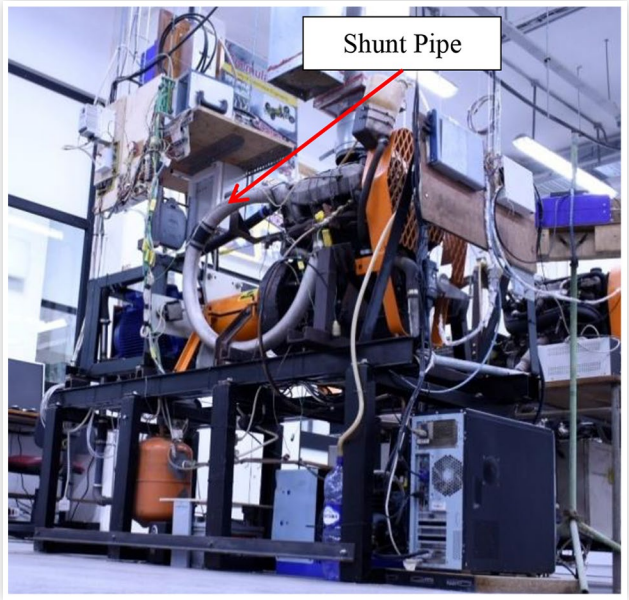

FIGURE 2 The instrumented locations on the cylinder head surface.

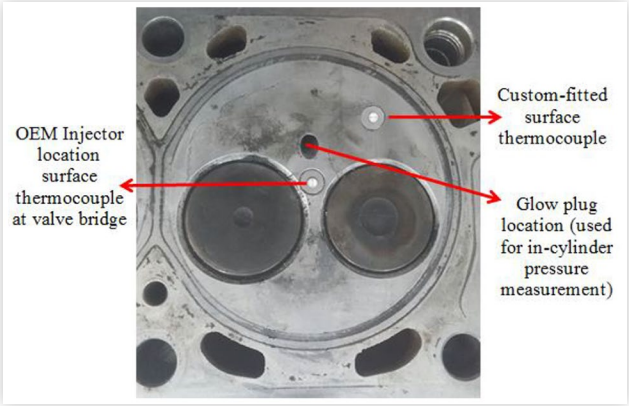

The eroding surface thermocouples that were used in this study were from Nanmac Corporation and are made up of two dissimilar thin metallic ribbons, which are physically separated by a 5 μm thin mica sheet. The sandwich is then placed between two cylindrical split-tapered inserts, but insulated by two mica sheets, one on each side. The combination is then pressed firmly into a hollow cylinder. The thermocouple junction is created by abrading the surface of the thermocouple with an emery cloth perpendicular to the metallic ribbons. A photo of the eroding thermocouple is shown in Figure 4, a microscope image of the surface of the thermocouple is shown in Figure 5 and an X-ray image of the thermocouple assembly is given in Figure 6. In total, four eroding thermocouples were used throughout this study, all of which were of ANSI type E, due to its high Seebeck EMF. Two of the used eroding thermocouples were of 1/8" diameter with

FIGURE 3 Locations on the piston crown that correspond to the cylinder head instrumented locations.

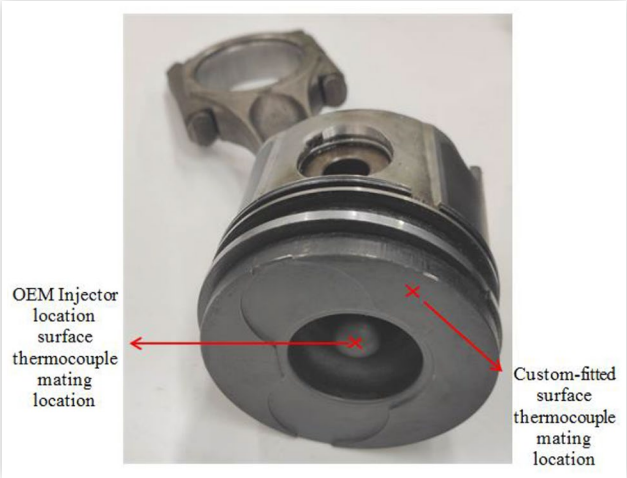

FIGURE 4 A photo of the eroding thermocouple.

FIGURE 5 A microscope image of the surface of the zirconia eroding thermocouple.

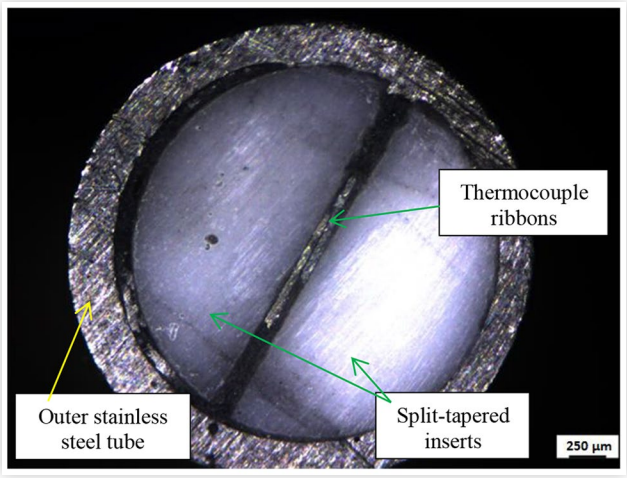

FIGURE 6 An X-ray image of the eroding thermocouple.

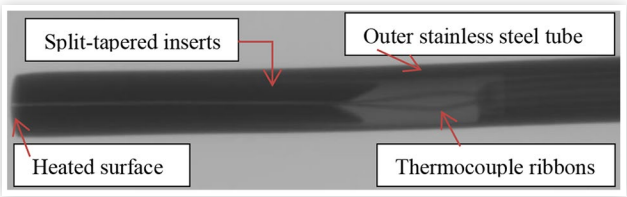

zirconia split-tapered inserts and stainless steel outer tube. Another thermocouple had stainless steel split-tapered inserts and 1/8" stainless steel outer tube, whereas the other thermocouple had aluminum split-tapered inserts and 1/4" aluminum outer tube. Note that data with all the mentioned thermocouples was obtained, however some of which is not presented in this publication for the sake of brevity.

The eroding thermocouples were procured with different split-tapered insert materials to study the multi-dimensionality of heat transfer, as detailed in [10]. It was found that both the aluminum and zirconia thermocouples show a very significant second dimension of heat transfer, whereas the stainless steel thermocouple exhibits two-dimensional heat transfer to a lower extent. One of the most prominent conclusions from [10] was that the heating timescale dictates which material of the thermocouple influences mostly the heat transfer, and hence a computation of the heat transfer using one set of thermophysical properties (density, specific heat capacity and thermal conductivity), as required by a one-dimensional heat transfer assumption, can never result in an accurate heat flux determination.

At the custom-drilled location in the cylinder head, one of the zirconia thermocouples was fitted throughout the test campaign. The other three thermocouples (zirconia, aluminum and stainless steel) were fitted in turns at the OEM injector location. When two-dimensional heat transfer was accounted for in the computation, it was found that the zirconia and stainless steel thermocouples at the OEM injector location gave very similar results at similar engine setpoints [10]. The aluminum thermocouple, at the same location, gave very high heat fluxes which are not conducive of a motored engine, hence results obtained from this thermocouple will be limited in this publication.

Obtaining the Heat Flux from Surface Temperature Measurements

The in-cylinder heat transfer at a given location on the cylinder head of the engine can be represented as the addition of two components; the time-invariant (steady-state) and the time-variant (transient) components of heat transfer. In this section, both of these components will be discussed separately since their methods of computation are different.

Obtaining the Time-Variant Component of Heat Transfer

The time-variant component of heat transfer is the one which is most computationally intensive. For this to be obtained, the surface temperature swing at the instrumented location is required. The surface temperature swing as recorded by the surface thermocouple cannot be represented by a simple mathematical function. As a result, in classical research, a Fourier series was used to represent the surface temperature swing after it was converted into the frequency domain by the use of the Fast Fourier Transform (FFT). In this case, the heat transfer problem was assumed to follow a one-dimensional approach through a semi-infinite solid. As discussed earlier in this paper, and detailed in [10], the heat flux through the eroding thermocouple is not truly one-dimensional. Hence, in modern research, methods which account for multi-dimensional heat transfer are being considered. In this research, the Impulse Response method was used with an impulse response function that was obtained from a two-dimensional finite element model of the different thermocouples used in this work. A detailed description of the method is given in [10], but a brief walkthrough of the method is presented below. The Impulse Response method for the processing of thermocouple surface temperatures was first introduced by Oldfield [16].

The impulse response method computes the time-variant component of heat transfer through a convolution between the surface temperature swing $T(t)$ and the impulse response function $h(t)$, as in equation (1). The impulse response function can be thought of as a function which has underlying information of how the surface temperature of the thermocouple responds for a known quantity of heat flux given to the surface of the thermocouple. Once the impulse response function for a given thermocouple is known, it can be convoluted with the measured surface temperature from engine experiments to give the time-variant heat flux at the instrumented location.

$$q''(t) = h(t) * T(t) \tag{1}$$

To obtain the impulse response function, a pair of basis functions $q_1''(t)$ and $T_1(t)$ are required. The basis function $T_1(t)$ may be, for example, the response of the thermocouple to a known step heat flux. There are three methods of how these basis functions may be obtained:

1. Analytical Models
2. Numerical Models
3. Characterization Experiments

Analytical models are often based on a one-dimensional, semi-infinite solid theory, given by equation (2), for a step heat flux $q_1''(t)$. This is unrealistic, in the same manner that the FFT method is, and hence not suggested. In fact, for a given temperature swing, the results of heat flux obtained from the FFT method and the Impulse Response method with a 1D impulse response function should be the same.

$$T_1(t) = \frac{2\, q_1''}{\sqrt{\rho c k}} \sqrt{\frac{t}{\pi}} \tag{2}$$

Numerical models may represent the thermocouple materials and three-dimensional geometry. This is often computationally intensive, but accounts for multi-dimensional heat transfer phenomena that cannot be captured by a one-dimensional method. In [10], Ansys® Academic Research Mechanical, Release 2019 R3 was used to set up a two-dimensional model of a plane surface of unit thickness. The model was made up of four different materials; two of which are the thermocouple dissimilar materials (ANSI type E), and the others are the Mica insulator, and the split-tapered insert material. A thermal transient analysis was done to find the temperature at the surface of the chromel ribbon in response to a 1 MW/m^2 step heat flux imposed to the surface. From this information of

$q_1''(t)$ and $T_1(t)$, the impulse response function $h(t)$ was found for every different thermocouple. The impulse response functions obtained in [10] were convoluted with the experimentally measured surface temperature swings from the engine obtained in this work, to determine the time-variant component of heat flux presented in the following section.

Characterization experiments offer the best results in terms of accuracy. This involves exposing the surface of the fast response thermocouple to a known heat flux originating from a focused laser beam, or shock wave experiments. As a result, with this method, apart from accounting for multi-dimensional effects, the impulse response function would also account for other physical uncertainties which cannot be included properly with a numerical model, for example the thermal resistance between the different materials of the eroding thermocouple.

Obtaining the Time-Invariant Component of Heat Transfer

The time-invariant component of heat transfer is often obtained by fitting a second thermocouple at a known recessed location, as close as possible to the axis of the surface thermocouple. The recess of the second thermocouple from the surface has to be such that the surface temperature swing at the recessed location is heavily attenuated [6]. The temperature gradient between the average surface temperature and the recessed temperature can be used in Fourier's law of one-dimensional conduction given by equation (3), to obtain the time-invariant component of heat flux.

$$q'' = -k\frac{dT}{dx} \tag{3}$$

There are several issues with using this method. The first is that it is often difficult to know the distance between the surface and the recessed thermocouple with good accuracy. Furthermore, it is known that the surface temperature as measured by the fast-response thermocouple is a function of the materials that make up the thermocouple. This means that the absolute temperature as measured by the surface thermocouple may not be the exact surface temperature of the cylinder head, had it not been disturbed. The thermal conductivity in equation (3) pertains to the material present between the surface temperature and the recessed temperature, hence that of the cylinder head. Since $\frac{dT}{dx}$ is however biased from the surface thermocouple materials, the use of equation (3) would render large numerical errors. Apart from the mentioned shortcomings, it was also reported that this method of obtaining the time-invariant component of heat transfer suffers greatly from multi-dimensional heat transfer due to the presence of coolant jackets and other features present in the cylinder head. Alkidas [17] reports a 20% error in the time-invariant component of heat transfer due to the presence of multi-dimensional heat transfer between the surface and recessed thermocouple. To avoid the presented errors associated with the time-invariant component of heat transfer, the recessed thermocouple method was not used in this research.

To have a more robust estimate of the time-invariant component of heat flux, a computation involving the 1st law of thermodynamics applied to the closed-part of the cycle of the motored engine was preferred, as given in equation (4). Equation (4) gives a crank-angle resolved heat flux, which if cycle-averaged gives an indication of the time-invariant component of heat flux. It is debatable if this can be added to the spatially-sensitive time-variant component as obtained from the Impulse Response method, since equation (4) is only capable of giving a zero-dimensional result. Furthermore, since equation (4) may only be implemented on the closed part of the cycle, this method assumes that the heat transfer during the intake and exhaust strokes is negligible. Although not strictly correct, this is a widely accepted assumption due to the relatively small temperature gradients between the gas and metal temperatures during the intake and motoring exhaust strokes.

$$-\frac{dQ}{dt} = p\frac{dV}{dt} + \frac{dU}{dt} \tag{4}$$

In equation (4), p is the instantaneous in-cylinder pressure and V is the instantaneous cylinder volume. For a motored engine, which experiences heat and blow-by losses, the in-cylinder pressure over the expansion stroke falls below the in-cylinder pressure over the compression stroke. Equation (4) combines the heat and blow-by loss in one term, $\frac{dQ}{dt}$, measured in *Watts*. To obtain the true heat flux from the cylinder, a correction to equation (4) had to be introduced. This correction was dealt with in detail by Pipitone in [18] and presented in equation (5), where m is the instantaneous trapped mass which decreases every crank angle due to blow-by. The introduced term involving $\frac{dm}{dt}$ represents the losses due to blow-by, hence $\frac{dQ}{dt}$ in equation (5) represents just the heat transfer from the gas to the cylinder. It should be noted that the ratio of specific heats, γ, in equations (4) and (5) is a function of the bulk gas temperature. Furthermore a sensitivity analysis on equation (5) revealed that the value and shape of $\frac{dQ}{dt}$ is heavily dependent on the accuracy of the compression ratio, in-cylinder pressure pegging and TDC phasing. In this research TDC phasing was obtained by using AVL OT-428 TDC probe. Pressure phasing was done by forcing a polytropic compression with a fixed polytropic exponent, according to [19].

$$-\frac{dQ}{dt} = \frac{\gamma}{\gamma-1}p\frac{dV}{dt} + \frac{1}{\gamma-1}V\frac{dP}{dt} - \frac{\gamma}{\gamma-1}\frac{pV}{m}\frac{dm}{dt}. \tag{5}$$

Overview of the Test Campaign

The experimental campaign conducted in this study was targeted at obtaining the in-cylinder surface temperature and resulting heat flux as a function of engine speed, pressure load (represented by peak of gas pressure), thermal load (represented by peak of in-cylinder bulk gas temperature) and coolant temperature. To conduct this analysis, four engine speeds were tested at 1400 rpm, 2000 rpm, 2500 rpm and 3000 rpm. The peak in-cylinder pressures (PCPs) tested were 40 bar, 60 bar, 80 bar and 100 bar. The coolant temperatures tested were 35°C,

60°C, 80°C and 95°C. The engine speed, PCP and coolant temperature were directly imposed by the controls of the setup. The peak of the bulk gas temperature was not directly imposed, but was varied by changing the operating gas. The gases tested were air, with a ratio of specific heats (γ) of 1.40, a mixture between oxygen, nitrogen and argon with γ of 1.50, a mixture between oxygen and argon with γ of 1.60 and argon gas with γ of 1.67. The indicative values of γ given here are quoted at atmospheric conditions. The change in variables presented above resulted in a large test matrix that cannot be effectively drawn here. The data shown in this publication is that which is deemed to be the most reliable and significant. All data obtained from this extensive test matrix is reported in [20].

Engine Experiments

In this section, the surface temperatures at the two instrumented locations, together with the computed heat fluxes are presented. The surface temperature and heat flux were first investigated with respect to engine speed, PCP and peak bulk gas temperature. Throughout this first test session, the engine coolant and oil temperatures were kept constant at 80°C. In a later test session, the effects of coolant temperature on surface temperature and heat flux are investigated.

The data for every test condition was measured when the engine was noted to reach steady-state conditions. The condition of steady-state was assessed by the settling of the coolant and oil temperatures within ±1 °C, PCP within around ±0.2 bar and engine speed within ±4 rpm. In cases where the gas used was not air, purging of the engine had to be done. Running the engine to steady-state conditions took an appreciable time of 5 to 10 minutes, depending on the testing sequence. The data presented in the fourth coming sections was obtained through an ensemble average over 300 cycles.

Despite the difficulties that in-cylinder heat transfer measurements present, it was found that both the surface temperature swing and heat transfer were relatively repeatable. Repeatability was assessed by running the engine at a "standard condition" of 1400 rpm, 80 bar PCP before and after the experimental test matrix. In both instances the surface temperature swing and time-variant component of heat flux were monitored and compared, since these are the most susceptible metrics to variances, due to the added complications of using the eroding surface thermocouples. It was found that the temperature swing varied by no more than 3 °C and the time-variant component of heat flux varied by no more than 0.3 MW/m^2 between the two tests. Figure 7 and Figure 8 report the temperature swing and time-variant component of heat flux respectively, at the standard test condition before and after completing a portion of the test campaign.

Surface Temperature and Heat Flux Variation with Engine Speed

The dependence of surface temperature and heat flux on engine speed is important due to its direct relation with cycle time, piston speed, and hence convective heat transfer coefficient. In this section, the PCP, gas composition and coolant/oil temperatures were kept constant while varying only the engine speed.

FIGURE 7 Ensemble surface temperatures taken at 1400 rpm, 80 bar PCP using air for repeatability evaluation. These temperatures were recorded by the Zirconia thermocouple fitted at the custom-drilled location.

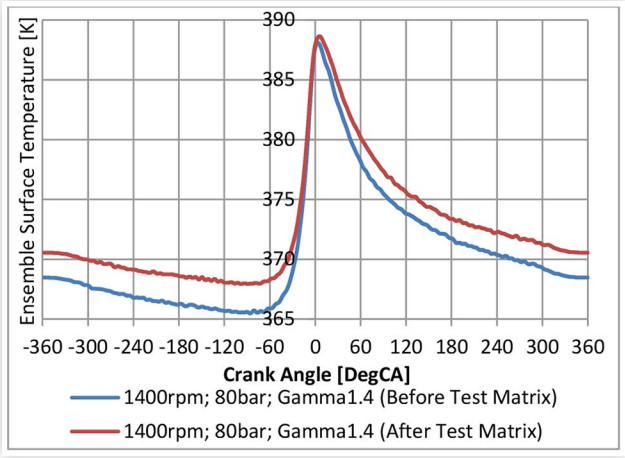

FIGURE 8 The time-variant component of heat flux at the custom-drilled location at 1400 rpm, 80 bar PCP and using air as the working gas.

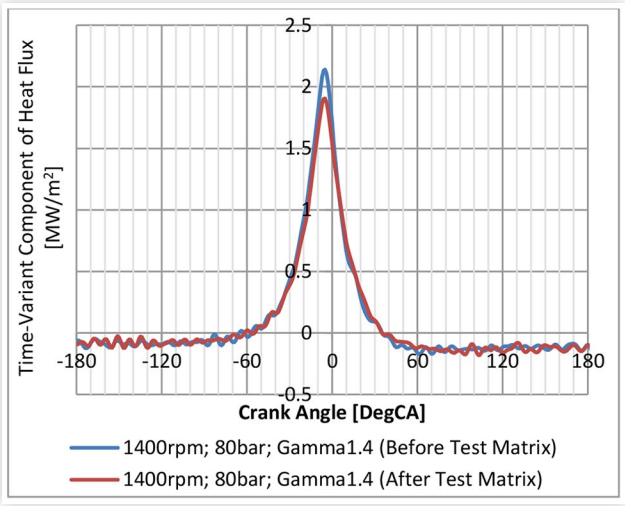

Figure 9 shows the cycle-average surface temperature recorded at the two instrumented locations. The OEM injector location was instrumented with the aluminum thermocouple, whereas the custom-drilled location was instrumented with the zirconia thermocouple. It should be noted that although the temperatures at both locations are plotted on the same graph, their comparison is not advisable since the temperatures recorded by each thermocouple are a function of the thermophysical properties of the thermocouple materials. In other words, had the aluminum and zirconia thermocouple been exposed to the same heat flux, the zirconia thermocouple would be expected to show a higher cycle-average surface temperature since zirconia has a lower diffusivity than aluminum. Since the cylinder head is made out of aluminum,

FIGURE 9 Cycle-average surface temperature against engine speed, using air as working gas.

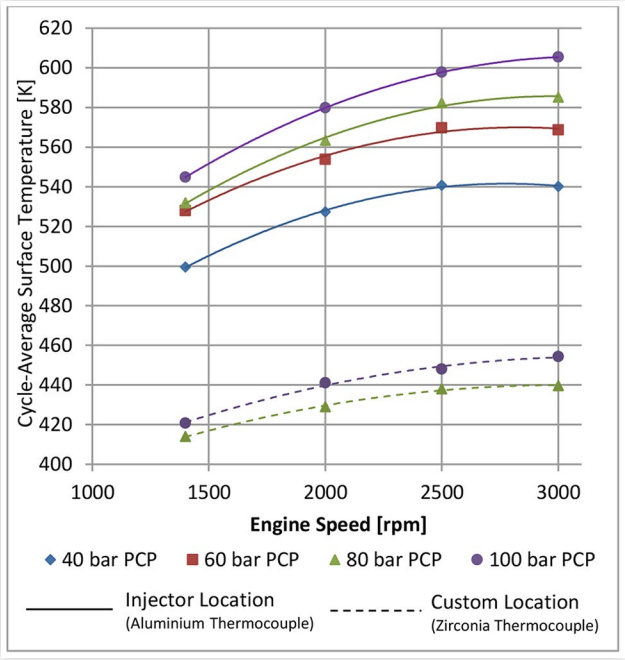

it is expected that the cycle-average surface temperature reported by the aluminum thermocouple is closer to the actual cylinder head surface temperature.

At both locations, the cycle-average surface temperature seems to show a diminishingly increasing trend with an increase in engine speed. For all PCPs considered, the graph shows saturation when increasing the engine speed from 2500 rpm to 3000 rpm. The saturation which is identified in this figure is one of interest and possibly a result of several interactions imposed by phenomena affected by the engine speed. Some of these effects may include: cycle time, cycle frequency, gas-side heat transfer coefficient and coolant-side heat transfer coefficient. It should be noted that throughout this research, the coolant was recirculated in the engine with an external electrical pump rotating at a fixed speed. The engine had its thermostat removed and water was used as the coolant fluid.

For the range of engine speed variation imposed in this research between 1400 rpm and 3000 rpm, an average increase of 50 K in the cycle-average surface temperature was noted, depending on the PCP of the setpoint. This is an expected result, since an increase in engine speed results in lesser time for heat to flow out of the cylinder, which hence results in a higher surface temperature.

The authors advise caution when observing the relationship of surface temperature with engine speed. With the experimental setup used in this research, the exhausted gas (in this case, air) was recirculated to the intake manifold. Due to this recirculation through the non-insulated, stainless steel shunt pipe, the intake gas temperature was different for every engine speed setpoint. The temperature of the gas at the intake side was measured by a K-type thermocouple and reported in Figure 10.

From the measured in-cylinder pressure, the bulk gas temperature could be computed over the valve-closed period, assuming the in-cylinder gas temperature at intake valve close

FIGURE 10 Intake gas temperature against engine speed, using air as working gas.

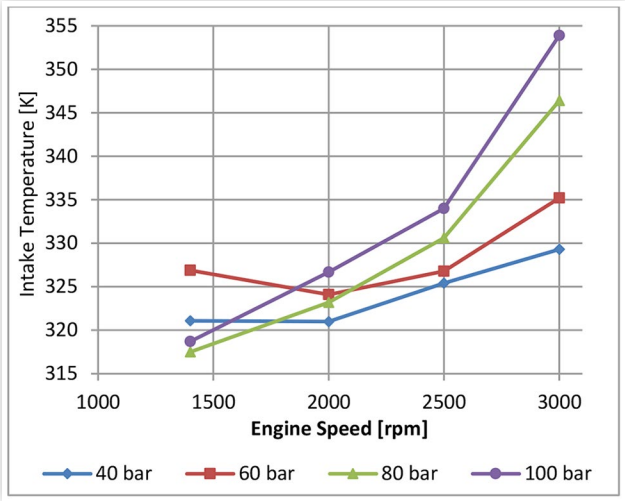

FIGURE 11 The computed peak bulk gas temperature against engine speed, using air as working gas.

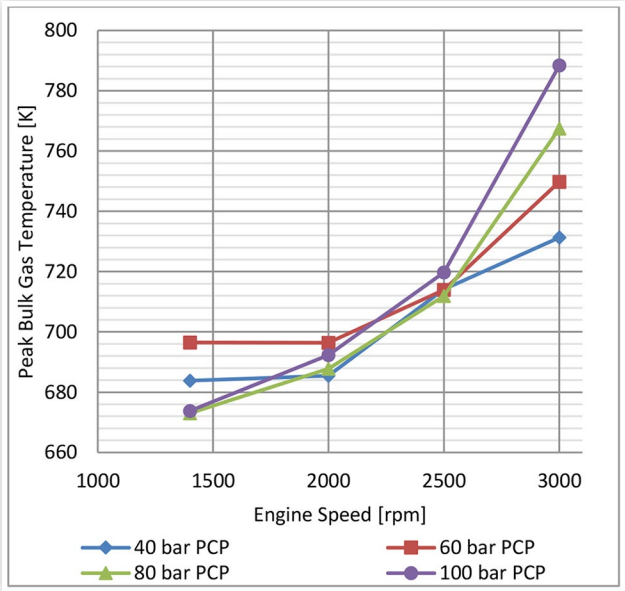

(IVC) to be equal to the measured intake gas temperature at the shunt pipe, and the in-cylinder gas pressure at IVC to be equal to the measured manifold absolute pressure (MAP). This computation assumes that no pressure and heat losses occur across the intake valve at IVC. Figure 11 shows that the peak bulk gas temperature increases with an increase in engine speed.

The time-invariant component of heat flux, as computed from the 1st law of thermodynamics (equation 5) is given in Figure 12, which also shows a diminishingly increasing trend with engine speed, similar to the trend presented earlier for surface temperature in Figure 9. It shall be pointed out that while Figure 9 was obtained through an experimental measurement from the eroding surface thermocouple, Figure 12 was obtained through a calculation using equation

FIGURE 12 The time-invariant heat flux against engine speed, obtained from the 1st law of thermodynamics, for air as operating gas.

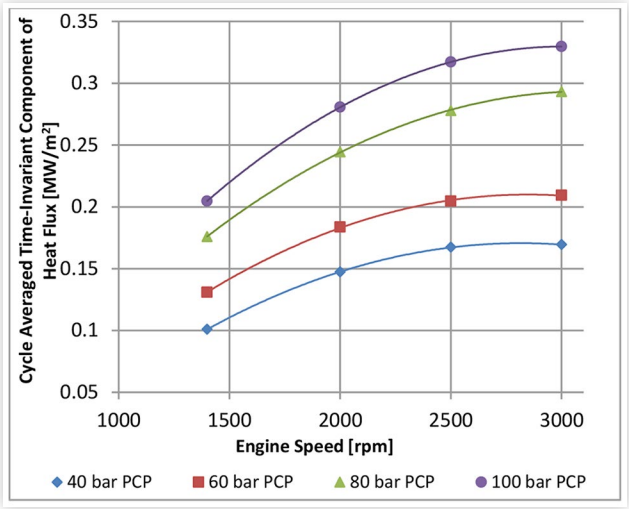

FIGURE 13 Ensemble surface temperature at 80 bar PCP, custom drilled location, and using air as working gas.

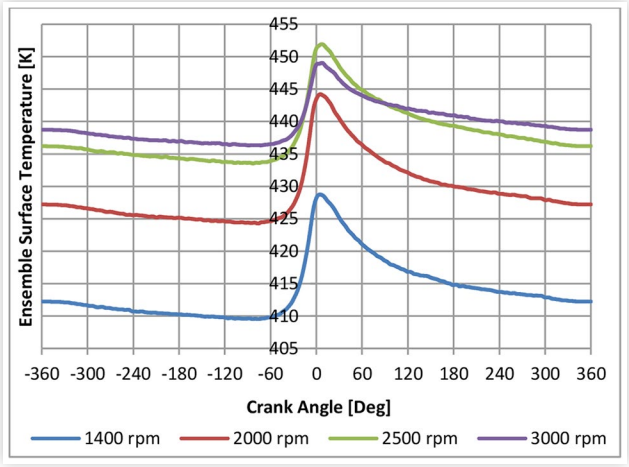

(5), from the experimentally measured in-cylinder pressure. The fact that the two graphs originate from different sources but show a similar trend, reinforces the observation being made. Increasing the engine speed from 1400 rpm to 3000 rpm showed an increase in the time-invariant component of heat flux between 40% and 65%, dependent on the PCP.

The measured surface temperature swing by the zirconia thermocouple at the custom-drilled location and computed time-variant component of heat flux are presented in Figure 13 and Figure 14 respectively. It is noted that the surface temperature swing and time-variant component of heat flux at the custom-drilled location do not show a progressive increase in their magnitude with engine speed. This could be a characteristic which is specific to the location of instrumentation. Since Figure 14 represents only the time-variant component of heat flux, and not the total, the reader may consult Figure 12 to have an approximate idea of the quantity by how much the graphs in Figure 14 should be shifted to get the total heat flux.

FIGURE 14 The time-variant component of heat flux against crank angle at 80 bar PCP, custom drilled location, and using air as working gas.

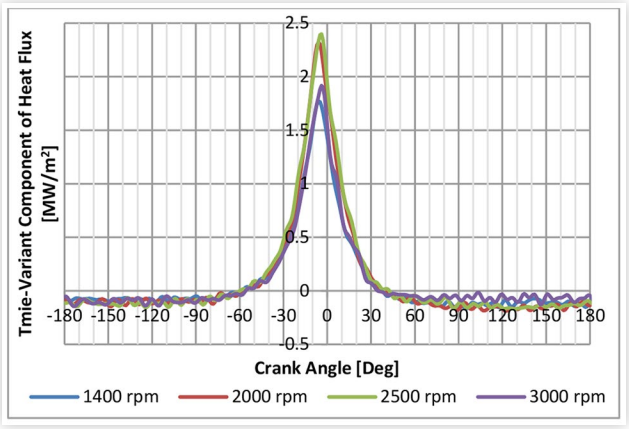

Surface Temperature and Heat Flux Variation with PCP

The surface temperature and heat flux variation with an increase in peak in-cylinder pressure is one of importance as it gives a measure of the thermal load variation with pressure load variation. In this section, the engine speed, gas composition and coolant/oil temperature were held constant while varying the PCP.

In a previous study by Torregrosa [8], in which the authors made use of pressurized motoring, it was reported that the average surface temperature, as well as total heat flux show a clear increase with an increase in PCP. This was also reported earlier by Overbye [1] and Annand [21].

Figure 15 shows the cycle-average surface temperature at the OEM injector location, recorded by the aluminium thermocouple. It is evident that an increase in PCP from 40 bar to 100 bar showed a quasi-linear variation in the surface temperature, with the gradient increasing with an increase in the engine speed. A similar variation was also noted in the time-invariant component of heat flux, as obtained from the 1st law of thermodynamics and presented in Figure 16. On average, increasing the PCP from 40 bar to 100 bar showed around 95% increase in the time-invariant component of heat flux.

The computed peak bulk gas temperature is presented in Figure 17 which shows that increasing the PCP from 40 bar to 100 bar shows very small changes in the peak bulk gas temperature, at all engine speeds. This is an expected result, and also thought to be one of the beneficial features of the pressurised motoring method. From theory, increasing the PCP in a motored engine should not induce a change in the peak bulk gas temperature, except for differences which arise from a different heat transfer rate or blow-by. This allows a decoupling of the gas pressure load effects from the gas thermal load effects on the studied metrics.

The temperature swing measured by the zirconia thermocouple at the custom-drilled location is given in Figure 18, while the computed time-variant component of heat flux is given in Figure 19. Varying the PCP from 80 bar to 100 bar at

FIGURE 15 Cycle-average surface temperature measured by the Aluminium thermocouple fitted at the OEM injector location, against a variation in PCP, using air as working gas.

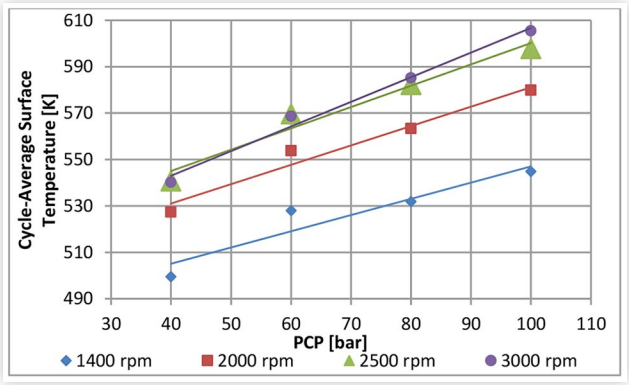

FIGURE 16 Time-Invariant component of heat flux as computed from the first law, against a variation in PCP, for air as working gas.

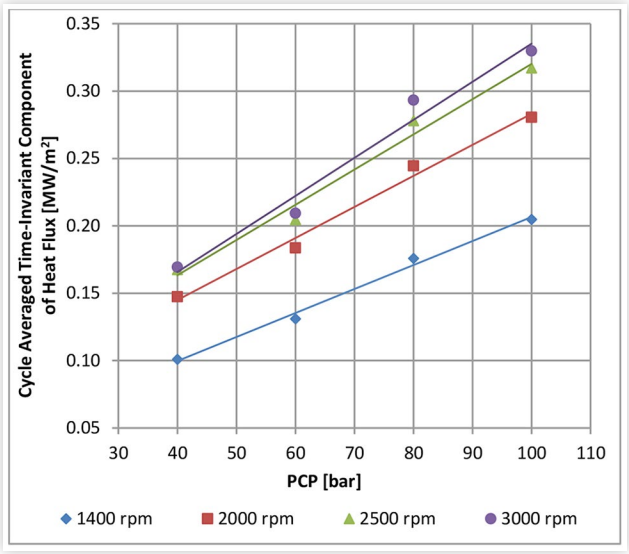

FIGURE 17 The computed peak bulk gas temperature against PCP, for air as working gas.

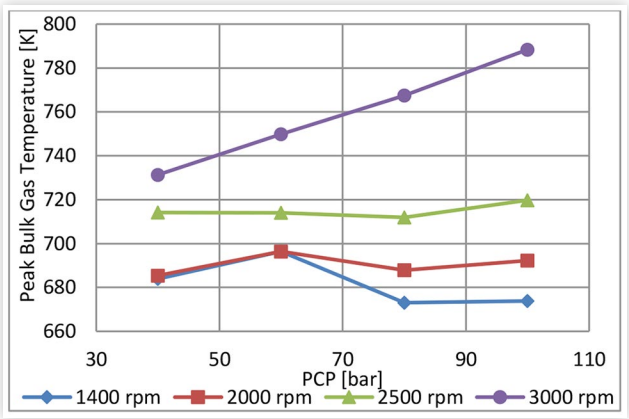

FIGURE 18 Ensemble surface temperature against crank angle, recorded by the Zirconia eroding thermocouple at the custom-drilled location at 1400 rpm, and using air as working gas.

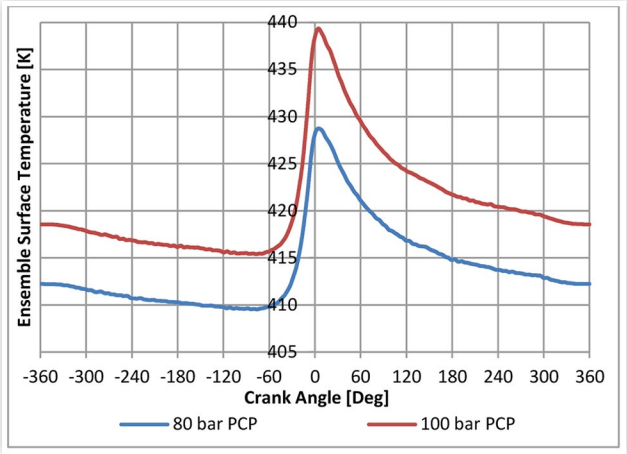

FIGURE 19 The time-variant component of heat flux against crank angle, at the custom-drilled location at 1400 rpm and using air as working gas.

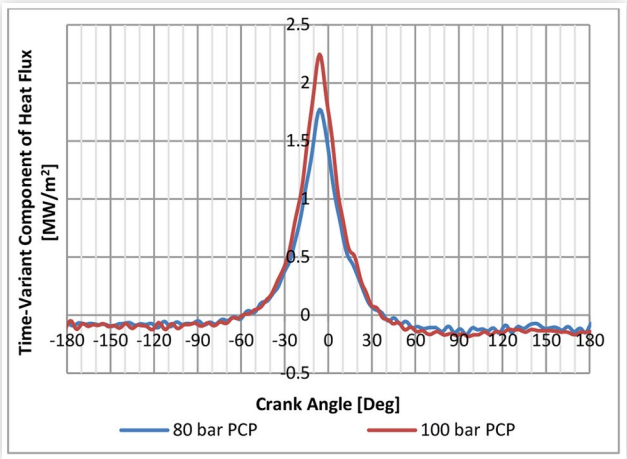

1400 rpm showed around 0.4 MW/m^2 increase in the transient component of heat flux at the peak, located at about 7 DegCA BTDC. It is noted that the change in the time-variant component of heat flux with a variation of PCP is only significant between 20 DegCA BTDC and 10 DegCA ATDC.

Surface Temperature and Heat Flux Variation with Bulk Gas Temperature

As presented in an earlier section, in this research, the bulk gas temperature was varied by motoring the engine with different gas compositions. This presented a very useful facility since the bulk gas temperature could be varied independently from the peak in-cylinder pressure. With this motored method, the effect on surface temperature and heat flux could

FIGURE 20 The computed peak of the bulk gas temperature for different working gases at 80 bar PCP.

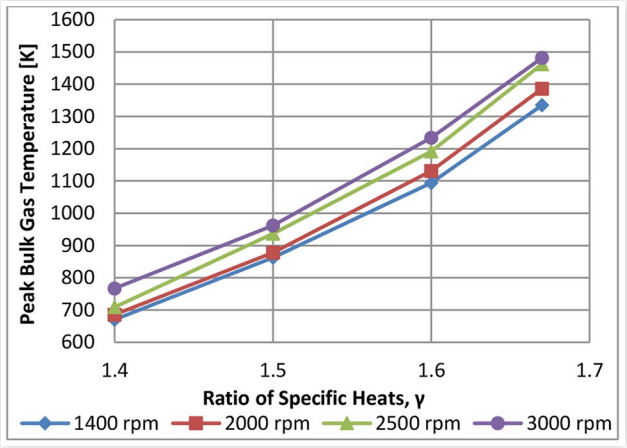

be studied with a drastic increase in the gas temperature, but without the presence of the gas dynamics instigated by combustion. In this section, the gas composition was varied, while the engine speed, PCP and coolant/oil temperatures were kept constant.

Figure 20 presents the peak of the computed bulk gas temperature for the four different working gases used on the pressurized motored setup. It should be noted that in some of the following graphs, the data for the gas mixture with γ of 1.67 is not presented since argon promoted heavy soot deposition on the surface thermocouples which was noted to slow down their response. This problem was also exhibited for the gas mixture of γ 1.6, which initially was being synthesized from oxygen, nitrogen and argon. The problem was traced down to the fact that the high gas temperatures reached with these gases were enabling the deterioration of the lubricant in the presence of an oxygen-deprived gas, which thus led to heavy soot deposits. To alleviate this problem, the gas mixture of γ 1.6 was then synthesized from just argon and oxygen. This resulted in a larger quantity of oxygen in the mixture which removed the problem of soot deposition. The gas mixtures of γ 1.5 and 1.4 (air) did not present such problem.

The cycle-average surface temperature recorded by the zirconia thermocouple at the custom-drilled location shows a linear variation with the peak bulk gas temperature, as presented in Figure 21. A linear variation was also noted between the time-invariant component of heat flux and the peak bulk gas temperature, presented in Figure 22. It is evident that the wall temperature shows a very small increase (45 K ~ 70 K) for a very large increase in the peak bulk gas temperature (600 K ~ 700 K). This large increase in the peak bulk gas temperature also resulted in about 35% to 50% increase in the time-invariant component of heat flux across the engine speed test spectrum.

Figure 23 and Figure 24 present the ensemble surface temperature and computed time-variant component of heat flux at the OEM injector location, as measured by the zirconia thermocouple. It is noted that the surface temperature of the zirconia thermocouple rises significantly when changing the

FIGURE 21 Cycle-average surface temperature obtained at the custom-drilled location by the Zirconia eroding thermocouple against the peak of the bulk gas temperature, at 80 bar PCP.

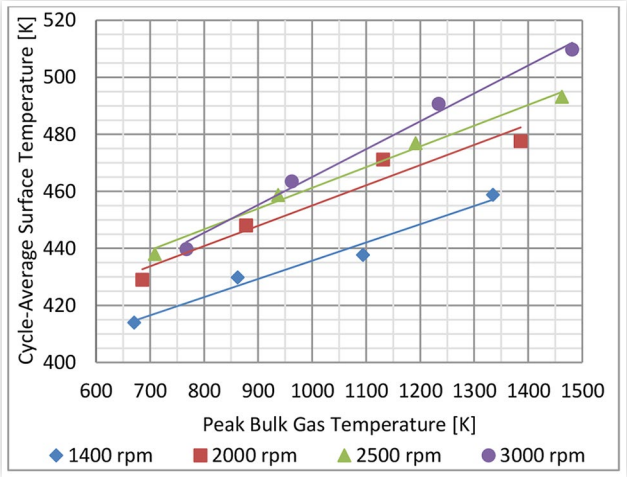

FIGURE 22 The time-invariant component of heat flux at different bulk gas temperatures at 80 bar PCP.

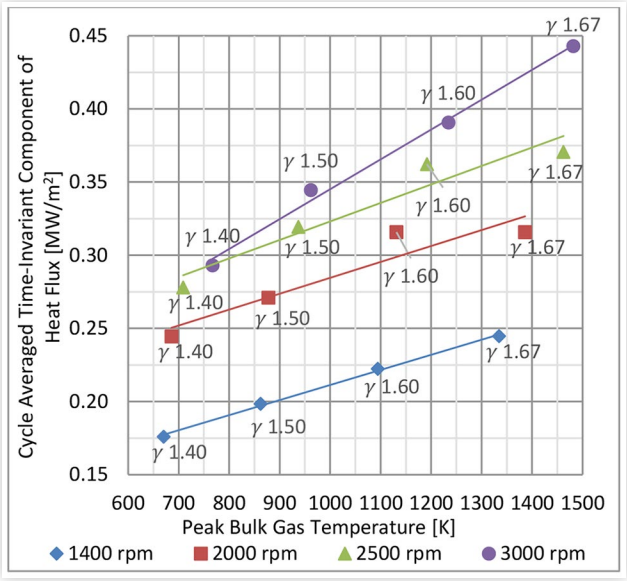

operating gas from air to the mixture of γ 1.6. The temperature swing also increases significantly which results in an increase in the time-variant component of heat flux, as shown in Figure 24. The difference in heat flux is mostly prominent in the region between 30 DegCA BTDC and 20 DegCA ATDC.

The observation noted at the OEM injector location contrasts with that made at the custom-drilled location for the same engine setpoints. Figure 25 and Figure 26 show the ensemble surface temperature and time-variant component of heat flux at the custom-drilled location, instrumented by the zirconia thermocouple. From these two figures it is visible that although the average value of ensemble surface

FIGURE 23 Ensemble surface temperature recorded by the zirconia thermocouple, fitted at the OEM injector location, at 3000 rpm.

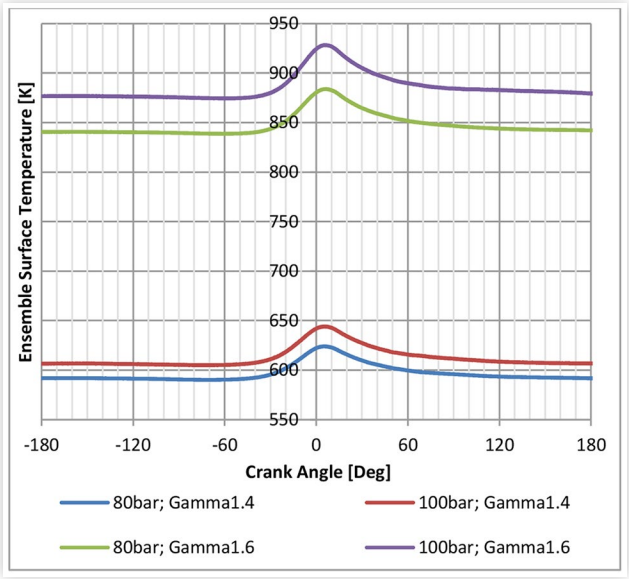

FIGURE 24 The time-variant component of heat flux at the OEM injector location, at 3000 rpm.

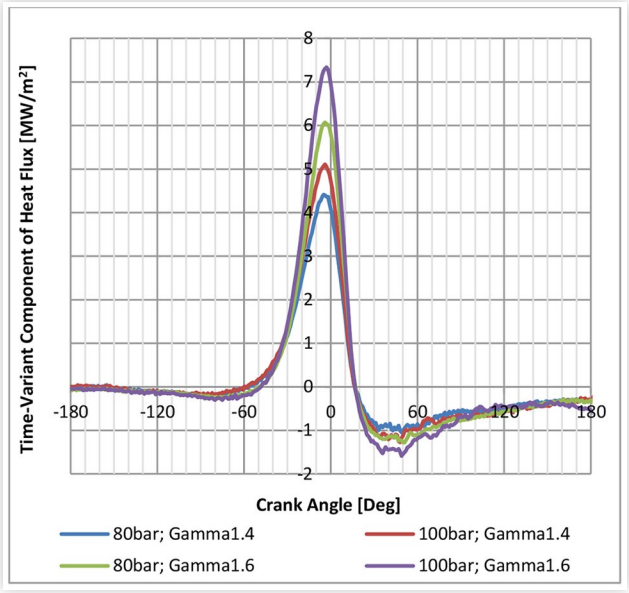

temperature increases when changing the gas mixture from γ 1.4 to 1.6, the temperature swing stays relatively constant. Consequently the transient component of heat flux varies only slightly.

By comparing Figure 23 with Figure 25, which were both instrumented by a zirconia thermocouple, it is evident that the thermocouple at the OEM injector location measured a much higher average surface temperature and slightly higher swing, than that at the custom-drilled location. This may

FIGURE 25 Ensemble surface temperature recorded by the zirconia thermocouple, fitted at the custom-drilled location, at 3000 rpm.

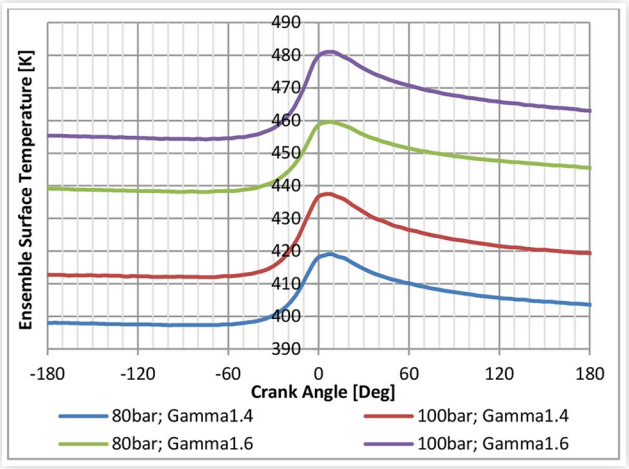

FIGURE 26 The time-variant component of heat flux at the custom-drilled location, at 3000 rpm.

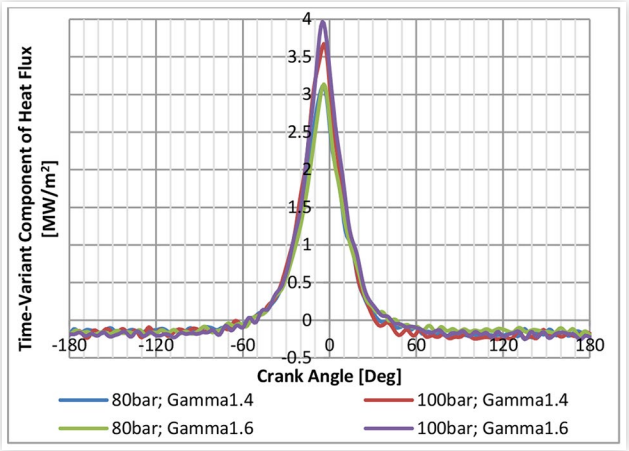

be attributed to the different gas dynamics that occur at the two locations, but it may also be a result of differences in the thermocouples assemblies, as explained in the experimental apparatus section.

Close observation of Figure 24 at the OEM injector location shows that the time-variant component of heat flux drops to a significant negative value just 20 DegCA ATDC, when the bulk gas temperature is still much higher than the measured wall temperature. This observation is well reported in literature and explained by the combined effects of the capacitive nature and compression work of the gas in the boundary layer [22]. Figure 26, measured at the custom-drilled location does not show this observation. It is thought that this difference may be explainable by the gas flow differences at the two locations, where at the OEM injector location a quiescent situation is expected, when compared to the high radial gas velocity expected at the custom-drilled location due to the presence of squish.

Surface Temperature and Heat Flux Variation with Coolant and Oil Temperature

Throughout all the previous sub-sections, the data reported was recorded at a constant coolant and oil temperature of 80°C. This was done mainly to reduce the variability in the surface temperature and heat flux which may be induced, mostly by the coolant temperature. In this section, the coolant/oil temperatures were varied while the engine speed, PCP and gas composition were held constant. To study the effect of the coolant and oil temperature on the surface temperature and heat flux, data will be presented for coolant and oil temperatures of 35°C, 60°C, 80°C, and 95°C.

Figure 27 presents the cycle-average surface temperature at the OEM injector location, as recorded by the aluminum thermocouple, which shows that the surface temperature increases linearly with an increase in the coolant and oil temperature. It is also noted that the gradients of the trendlines are very close to unity, meaning that the surface temperature increased by a similar quantity to the increase in the coolant and oil temperature.

The computed peak bulk gas temperature at 3000 rpm and 80 bar PCP is given for different oil/coolant temperatures in Figure 28, along with the corresponding intake temperatures for each test. It is shown that increasing the oil/coolant temperature showed an increase in the peak bulk gas temperature. The shape of variation of peak bulk gas temperature with engine speed is shown to be similar to the shape of variation of the intake gas temperature with engine speed.

The time-invariant component of heat flux is presented in Figure 29 at 80 bar PCP. It shows that for the engine tested in this research, an increase in the coolant and oil temperature from 35°C to 95°C rendered almost a negligible change in the time-invariant component of heat flux. It should be noted that whilst the variation in coolant/oil temperature imposed in this research seems large, it is still insignificant when compared to the gas side temperatures that go up to 550 °C when using air and 1200 °C when using Argon. This provides a reasonable explanation to the negligible change observed in the time-invariant component of heat flux when changing the coolant/oil temperature from 35 °C to 95 °C. Furthermore, the variation in the coolant/oil temperature imposed, even though significant at the coolant side, it is not enough to significantly change the coolant/oil properties which govern the coolant-side heat transfer coefficient.

To summarize the results section, Table 2 is presented with a brief summary of all the results introduced earlier in this section, according to the controlled variable.

FIGURE 27 Cycle-average surface temperature measured by the Aluminum thermocouple at the OEM injector location with a variation in the coolant and oil temperatures at 80 bar PCP and using air as working gas.

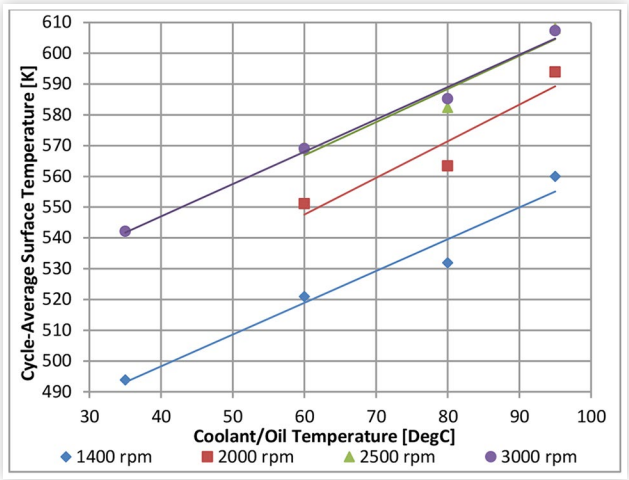

FIGURE 28 The computed peak bulk gas temperature at different oil and coolant temperatures, at 3000 rpm; 80 bar PCP and using air as the working gas.

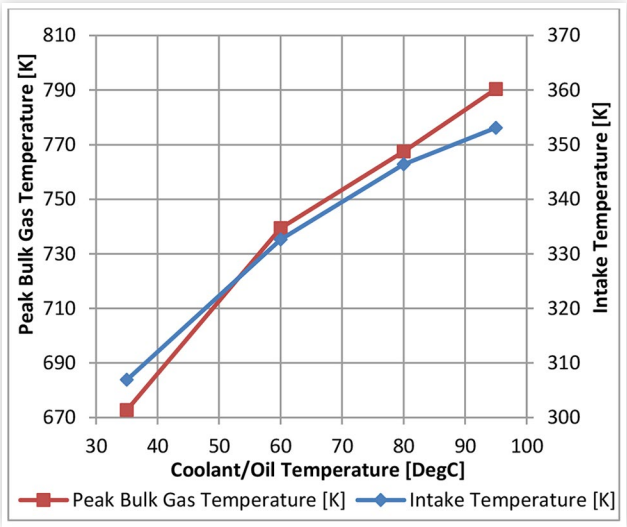

FIGURE 29 The time-invariant component of heat flux obtained from the 1st law of thermodynamics at different coolant/oil temperatures for air as the working gas.

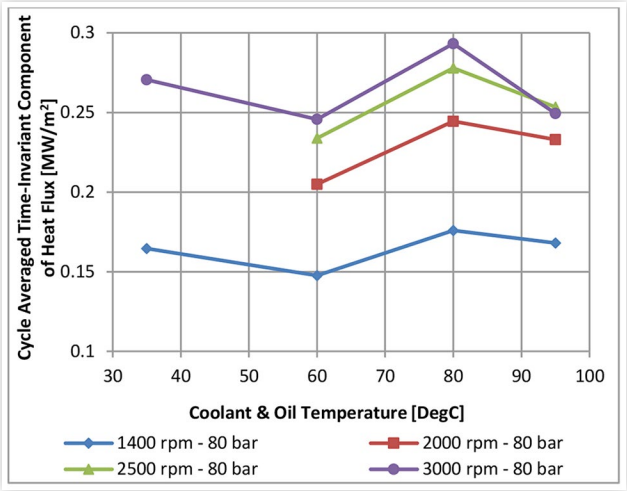

TABLE 2 Summary of presented results.

		Peak of Bulk Gas Temp.	Mean Surface Temp.	Time-Invariant Component of Heat Flux	Time-Variant Component of Heat Flux
Variable Increasing	*Engine Speed*	Increased	Diminishingly increasing trend with saturation	Diminishingly increasing trend with saturation	Non-consistent increase around the peak
	PCP	Relatively constant	Increased linearly	Increased Linearly	An evident increase close to the peak
	Gas Compos.	Increased Linearly	Increased Linearly	Increased Linearly	Increased significantly at injector location, and increased only slightly at custom-drilled location
	Coolant and Oil Temp.	Increased	Increased linearly with a gradient of unity	Insignificant Effect	-

Conclusions

In this research, a parametric study on in-cylinder surface temperature and heat flux was carried out, investigating the effect of engine speed, peak in-cylinder pressure, peak in-cylinder bulk gas temperature and coolant/oil temperatures. The surface temperature was obtained by fitting two fast response thermocouples of the eroding type; one at the cylinder central location, and another at the cylinder periphery in the squish region. The method used to obtain the time-variant component of heat flux from the surface temperature swing was the Impulse Response method taking into account two-dimensional heat flux through the thermocouple. The time-invariant component of heat flux was computed from a zero-dimensional approach using the first law of thermodynamics, with a correction term accounting for the blow-by loss. From this research the following conclusions were drawn:

1. Engine Speed Effect - Experimental results obtained at the OEM injector location and custom-drilled location showed that an increase in the engine speed results in a diminishingly increasing trend in the cycle-average surface temperature and the time-invariant component of heat flux, with saturation occurring at high speeds of 3000 rpm. Changing the engine speed showed only a small increase in the time-variant component of heat flux.
2. PCP Effect - An increase in PCP showed a linear increase in the cycle-average surface temperature, a linear increase in the time-invariant component of heat flux and a moderate increase in the time-variant component of heat transfer.
3. Gas Composition Effect - Using gases with ratios of specific heats ranging from 1.40 to 1.67 (at room temperature) resulted in peak bulk gas temperatures of 700 K to 1500 K. This considerable increase in the peak bulk gas temperature, at a constant PCP, resulted in a significant linear increase in the cycle-average surface temperature at both instrumented locations, and a linear increase in the computed time-invariant component of heat flux. Increasing the peak of the bulk gas temperature also showed a relatively large increase in the time-variant component of heat flux at the OEM injector location (central location), but only a small change in the time-variant component of heat flux at the custom-drilled location (cylinder periphery - squish region).
4. Coolant and Oil Temperature Effect - The coolant and oil temperatures were varied from 35°C to 95°C. These showed a linear increase in the cycle-average surface temperature with a gradient of unity. The computed time-invariant component of heat flux was not significantly affected. This was attributed to the small temperature change induced in the coolant/oil when compared to the high gas temperatures reached due to compression.
5. From the four tested variables, engine speed, PCP, bulk gas temperatures and coolant/oil temperature, it was found that the PCP had the most significant effect on the time-invariant component of heat flux. All tested variables had significant impact on the cycle-average surface temperature. The surface temperature swing and time-variant component of heat flux were affected by all tested variables, but the clearest variation was noted with a variation in PCP.
6. It was found that the cycle-average surface temperature and time-variant component of heat flux at the OEM injector location showed larger magnitudes than that experienced at the custom-drilled location for the same engine setpoint, when both locations were instrumented by the same zirconia thermocouple. It is thought that this could be a result of the tumbling motion of the gas close to the central axis of the cylinder, but it could also potentially be a result of local flow disturbances at the OEM injector location arising from the fitment of the surface thermocouple.

The six conclusions outlined above were obtained from a pressurized motored engine operated with different working gases. This implies that the conclusions drawn do not necessarily readily represent the conventional fired production engine due to the different operating environment. This study, however, has obtained the relationship of surface temperature and heat flux with individual variations of four different variables, two of which having high importance and less researched than others; thermal load (variation of peak bulk gas temperature) and pressure load (variation of PCP). This research, therefore, provides a good basis against which a

one-dimensional model can be fine-tuned. If the model can be made to match the experimentally obtained data, it would then have to bridge a smaller gap to be upgraded to model the production fired engine.

Suggestions for Further Work

Now that an extensive parametric data set was obtained with good repeatability from the pressurized motored engine, it would be of benefit if an interested simulation analyst would undertake the exercise of modeling the engine tested experimentally in this work and tune the model to match the experimental results reported in this publication. This exercise will definitely be challenging, however the test session presented was aimed at segregating the effects imposed on surface temperature and heat transfer by engine speed, PCP, gas composition and coolant/oil temperature, which hence should provide for a solid foundation for building the model.

References

1. Overbye, V., Bennethum, J., Uyehara, O., and Myers, P., "Unsteady Heat Transfer in Engines," SAE Technical Paper 610041 (1961), doi:10.4271/610041.
2. Lucht, T.P., Dunn-Rankin, D., Walter, T., Dreier, T. et al., "Heat Transfer in Engines: Comparison of Cars Thermal Boundary Layer Measurements and Heat Flux Measurements," SAE Technical Paper 910722 (1991), doi:10.4271/910722.
3. Wang, X., Stone, R., Stevens, R., Arita, Y. et al., "Finite Element Analysis of Eroding Type Surface Thermocouple with Application to Engine Heat Flux Measurement," SAE Technical Paper 2006-01-1045 (2006), doi:10.4271/2006-01-1045.
4. Buttsworth, D.R., "Transient Response of an Erodable Heat Flux Gauge using Finite Element Analysis," *Proceedings of the Institution of Mechanical Engineers, Part D: Journal of Automobile Engineering* 216, no. 8 (2002): 701-706.
5. Hennes, C., Lehmann, J., and Koch, T., "Possibilities of Wall Heat Transfer Measurements at a Supercharged Euro VI Heavy-Duty Diesel Engine with High EGR-Rates, an In-Cylinder Peak Pressure of 250 Bar and an Injection Pressure up to 2500 Bar," SAE Technical Paper 2019-24-0171 (2019), doi:10.4271/2019-24-0171.
6. Alkidas, A.C., "Heat Transfer Characteristics of a Spark-Ignition Engine," *Journal of Heat Transfer* 102 (1980): 189-193.
7. Hoag, K., "Measurement and Analysis of the Effect of Wall Temperature on Instantaneous Heat Flux," SAE Technical Paper 860312 (1986), doi:10.4271/860312.
8. Torregrosa, A.J., Bermúdez, V., Olmeda González, P.C., and Figueroa Garcia, O.L., "Experimental Assessment for Instantaneous Temperature and Heat Flux Measurements under Diesel Motored Engine Conditions," *Energy Conversion and Management* 54, no. 1 (2012): 57-66.
9. Annand, W.J.D. and Ma, T.H., "Instantaneous Heat Transfer Rates to the Cylinder Head Surface of a Small Compression-Ignition Engine," *Proceedings of the Institution of Mechanical Engineers* 185 (1970): 976-987.
10. Caruana, C., Farrugia, M., Mollicone, P., Pipitone, E. et al., "In-Cylinder Heat Transfer Determination Using Impulse Response Method with a Two-Dimensional Characterization of the Eroding Surface Thermocouple," SAE Technical Paper 2021-24-0018 (2021), doi:10.4271/2021-24-0018.
11. Caruana, C. and Farrugia, M., "Balancing of a Four Cylinder Engine for Single Cylinder Operation," in *19th Mechatronika IEEE Conference*, Prague, Czech Republic, 2020.
12. Caruana, C., Farrugia, M., and Sammut, G., "The Determination of Motored Engine Friction by Use of Pressurized 'Shunt' Pipe between Exhaust and Intake Manifolds," SAE Technical Paper 2018-01-0121 (2018), doi:10.4271/2018-01-0121.
13. Caruana, C., Farrugia, M., Sammut, G., and Pipitone, E., "Further Experimental Investigation of Motored Engine Friction Using Shunt Pipe Method," *SAE Int. J. Adv. & Curr. Prac. in Mobility* 1, no. 4 (2019): 1444-1453, doi:10.4271/2019-01-0930.
14. Caruana, C., Farrugia, M., Sammut, G., and Pipitone, E., "Experimental Investigation on the Use of Argon to Improve FMEP Determination through Motoring Method," SAE Technical Paper 2019-24-0141 (2019), doi:10.4271/2019-24-0141.
15. Caruana, C., Farrugia, M., Sammut, G., and Pipitone, E., "Further Experiments on the Effect of Bulk In-Cylinder Temperature in the Pressurized Motoring Setup Using Argon Mixtures," *SAE Int. J. Adv. & Curr. Prac. in Mobility* 2, no. 4 (2020): 2142-2155, doi:10.4271/2020-01-1063.
16. Oldfield, M.L.G., "Impulse Response Processing of Transient Heat Transfer Gauge Signals," *Journal of Turbomachinery* 130, no. 2 (2008): 021023, doi:10.1115/1.2752188.
17. Alkidas, A.C., "Thermal Loading of the Cylinder Head of a Spark Ignition Engine," *Heat Transfer Engineering* 3, no. 3-4 (1982): 66-75, doi:10.1080/01457638108939585.
18. Pipitone, E. and Beccari, A., "Determination of TDC in Internal Combustion Engines by a Newly Developed Thermodynamic Approach," *Applied Thermal Engineering* 30, no. 14-15 (2010): 1914-1926.
19. Randolph, A.L., "Methods of Processing Cylinder-Pressure Transducer Signals to Maximize Data Accuracy," SAE Technical Paper 900170 (1990), doi:10.4271/900170.
20. Caruana, C., "Incylinder Heat Transfer and Friction Analysis in Pressurised Motored Compression Ignition Engine," PhD dissertation, University of Malta, Malta, 2020.
21. Annand, W.J.D. and Pinfold, D., "Heat Transfer in the Cylinder of a Motored Reciprocating Engine," SAE Technical Paper 800457 (1980), doi:10.4271/800457.
22. Wendland, D.W., "The Effect of Periodic Pressure and Temperature Fluctuations on Unsteady Heat Transfer in a Closed System," NASA Report 72323, 1968.

Contact Information

Mario Farrugia
Mechanical Engineering Department, University of Malta, Malta
Email: mario.a.farrugia@um.edu.mt

Carl Caruana
Mechanical Engineering Department, University of Malta, Malta
Email: carl.caruana.12@um.edu.mt

Acknowledgments

Prof. Martin Oldfield from Oxford University is thanked for his guidance in using the impulse response method, together with sharing his MATLAB scripts.

The research work disclosed in this publication is partially funded by the Endeavour Scholarship Scheme (Malta). Scholarships are part-financed by the European Union-European Social Fund (ESF)-Operational Programme II-Cohesion Policy 2014-2020 "Investing in human capital to create more opportunities and promote the well-being of society".

Definitions/Abbreviations

AL - Aluminum
ATDC - After Top Dead Centre
BBDC - Before Bottom Dead Centre
BTDC - Before Top Dead Centre
CA - Crank Angle
CAD - Crank Angle Degrees
CARS - Coherent Anti-Stokes Raman Scattering
EVO - Exhaust Valve Opened
FEA - Finite Element Analysis
FFT - Fast Fourier Transform
HDi - High-Pressure Direct Injection
IR - Impulse Response
IVC - Intake Valve Closed
OEM - Original Equipment Manufacturer
OHC - Overhead Camshaft
PCP - Peak In-Cylinder Pressure
SI - Spark Ignition
SS - Stainless Steel.

e-ISSN 2641-9645